Load-Frequency Control in a Two-Area Power System Using the Fuzzy-PID Method

Saeed Gerami Moghaddam[1], **Ali Asghar Bagheri**[2], and **Reza Sedaghati**[3†], Non-members

ABSTRACT

Power systems are plant units connected to each other, with the electrical power flow constantly moving between them and the load. All systems must be implemented in such a way that they remain stable not only under normal conditions but also after the implementation of unwanted inputs or malfunctions and should be able to return to stable nominal conditions as soon as possible. The basic factors of stability control in a power system are the frequency of different areas and the amount of power flow between them. Now that the main goals of stability control in a power system have been stated, these indicators must be kept at their desired levels through the design and implementation of controllers. This paper first describes the mechanism of load frequency control (LFC). The parameters of several types of complementary controllers are then designed based on the proposed algorithm. The controllers designed on the simulated power system are finally applied, and the effect of each controller on faster damping of frequency fluctuations is discussed. In this study, a multi-area power system is simulated and the effect of disturbance in each area and the performance of the proposed controller in controlling the frequency of the whole network are investigated. The case studies show that the share of active and reactive power generation sources in each region have the greatest impact on frequency control, given that the proposed control coefficients are determined using fuzzy logic in the shortest possible time and the number of transient oscillations eliminated, resulting in a steady system.

Keywords: Load-Frequency Control, LFC, Fuzzy Method, Two-Area Fuzzy System

1. INTRODUCTION

The load frequency control (LFC) issue has been widely debated for over three decades. On the other hand, power systems are generally large and have nonlinear dynamics. However, the intention was to solve the LFC problem in simple mode, using a two- or multi-area power system in linear mode. These nonlinear behaviors in the power system and the problems arising from its simple and linear state are described in detail by the authors of [1–3]. Moreover, the effects of generation rate constraints (GRCs; amount of imposed power generation) on the outputs, both in continuous and discrete time, have been examined in several studies including [4, 5].

Initial efforts to address the LFC problem involved controlling the frequency of the power system through the governor itself and the related flywheel. This mechanism gradually failed and to solve the above problem (damping in oscillations with very long times) an additional control process was added by the governor using a signal proportional to the amount of frequency deviation and its integral. Thus, a classical answer to the solution of the LFC problem was gradually formed.

Considering previous studies such as [6–8], it can be observed that the "centralized control procedure" is used to solve the LFC problem. If greater attention is paid to the subject, the method of "centralized" control can be observed to require the exchange of information from the "control areas" to all fields of the power system, which are geographically very far apart. Furthermore, this type of control mode requires complex calculations and the results are difficult to store.

Thus, a concept emerged based on a "decentralized control strategy" to respond efficiently to the LFC problem. As a result, many studies have used the "decentralized control strategy" to solve the problem of LFC in continuous and discrete mode [9, 10]. The work of [9] also presents the design of a controllable and visible power system with a decentralized control strategy in which the control feedback loops are completely independent of each other.

Classical control methods for solving the LFC problem are those in which the error signal is constructed based on the control error integral. In the classical control method, a diagram is obtained to achieve the desired "gain limit (K_m)" and "phase margin (φ_m)" with the Nyquist curve used as the reference geometry location. This makes this type of controller complex and the design process slow. Although these types of controllers are

Manuscript received on March 18, 2022; revised on July 31, 2022; accepted on October 12, 2022. This paper was recommended by Associate Editor Matheepot Phattanasak.

[1]The author is with the Department of Electrical Engineering, Kharg Branch, Islamic Azad University, Kharg, Iran.

[2]The author is with the Department of Electrical Engineering, Dashtestan Branch, Islamic Azad University, Dashtestan, Iran.

[3]The author is with the Department of Electrical Engineering, Beyza Branch, Islamic Azad University, Beyza, Iran.

[†]Corresponding author: sedaghati.r@biau.ac.ir

Digital Object Identifier: 10.37936/ecti-eec.2023211.248665

reliable and simple to implement, according to the results obtained in [11–14], power systems with such controllers exhibit poor dynamic performance. In addition, these control systems are inefficient when the power system is repeatedly exposed to disturbances, changes in parameters, or nonlinear events. Nevertheless, the complexity of adaptive controllers, along with the many recurring problems that can occur in a power system, prevent such controllers from performing their primary role in resolving the LFC problem. In addition, since these types of controllers are based on the equations of state in a linearized model, the control process may require the prediction of out-of-reach state variables.

With the increasing penetration of renewable energies in power systems, the issue of frequency control has become more important, and conventional control methods are unable to maintain the stability of the power system. In smart grids, demand response as a frequency control tool reduces the grid's dependence on rotating storage and high-cost controllers. In addition to the economic benefits of load response, the damping of high-speed frequency changes is one of its important features. In [15], the frequency control of an islanded microgrid is presented, using intelligent load response control based on fuzzy logic and a particle swarm optimization algorithm. It has the ability to continuously balance production and demand despite natural and uncertain changes in the output power of resources, providing wind and solar energy.

In [16], the imperial competition algorithm (ICA) and the integral time-absolute error (ITAE) criterion are used to optimally adjust the load frequency of PID controller parameters in two-zone power systems, taking account of the changes in the power system parameters. In order to achieve the desired robust performance, it is important to consider the appropriate objective function to demonstrate that by using the ITAE criterion, (despite the frequency deviation and control area error), the optimal control parameters for the power system can easily be obtained from the colonial competition algorithm, which has high accuracy and convergence speed.

Since the islanding power system, including renewable resources, faces stability problems due to the lack of interaction between the production and consumption power, power fluctuations in the network can cause serious problems. Frequency control is very important in the operation of microgrids, and if this is not achieved, even in the case of a proper design, the microgrid is still likely to face unforeseen problems. In [17], a new combination of photovoltaics, a wind turbine, storage, and load on the consumer side are used, controlled using fuzzy logic, and the particle swarm optimization algorithm to improve the controller.

The rapid growth and penetration of microgrids and their other capabilities, including load response, are responsible for LFC being different from traditional methods. Presenting new methods of frequency control in such systems has always been of interest to researchers. Therefore, in [18], the three-zone power system based on a DFIG microgrid and hydrogen energy storage is investigated in addition to load response from the perspective of frequency load, with a genetic algorithm used to improve performance.

Therefore, the method presented in this paper, while eliminating the shortcomings mentioned in the introduction, can be easily coded to maintain stability in the two-area power system. Determining the controller coefficients by a fuzzy algorithm not only reduces the number of overshoots but also the settling time while limiting the sudden increase in the signal ascent time to achieve a lasting response.

This paper is structured as follows: Section 2 presents the concept of LFC and its formulation. The fuzzy optimization algorithm is discussed in Section 3. The various simulations and case studies on the two-area power network are presented in Section 4, demonstrating the superiority of the proposed algorithm. Finally, Section 5, provides the study results.

2. PROBLEM FORMULATION

In this section, a single generator is first modeled to feed a local power supply area by considering the appropriate assumptions and approximations. The study then extends to several generators, all part of the same area. The connection between power areas is then examined.

2.1 Generator Model

The oscillation equation of a synchronous machine for small perturbation is mathematically represented in Eq. (1) [19].

$$\frac{2H}{\omega_s}\frac{d\Delta\omega}{dt} = \Delta P_m - \Delta P_e \tag{1}$$

where H is the inertia constant of the machine at the base power of the system, whereas ΔP_m and ΔP_e are the mechanical input power and electrical output power of the generator, respectively. The angle of power in terms of electric radians and ω_s represents the angular velocity in terms of electric radians per second. The small deviation in velocity is written as

$$\frac{d\Delta\omega}{dt} = \frac{\omega_s}{2H}\left(\Delta P_m - \Delta P_e\right) \tag{2}$$

and putting frequency instead of angular velocity gives:

$$\frac{d\Delta f}{dt} = \frac{f_s}{2H}\left(\Delta P_m - \Delta P_e\right) \tag{3}$$

where f_s is the nominal frequency of the system in Hz. By taking the Laplace transform from both sides of the above relation and arranging it, the block display for the generator is shown in Fig. 1.

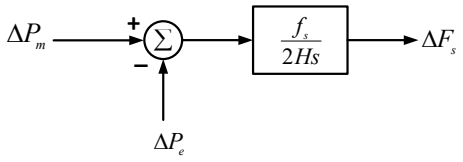

***Fig. 1**: Block diagram of the generator model.*

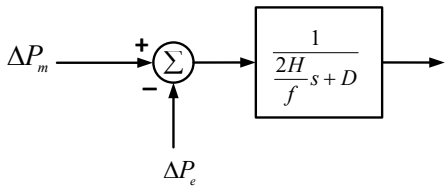

***Fig. 2**: Block diagram of the generator and load model.*

2.2 Load Model

The load of a power system includes a wide range of electrical devices that are independent of frequency for resistive loads such as light and heat. However, motor loads are sensitive to changes in frequency, and their level of sensitivity depends on the combination of load characteristics and speeds.

Considering the velocity characteristics of a combined load $D\Delta\omega$, the frequency-sensitive load changes show that the parameter D is obtained from Eq. (4) [20].

$$D = \frac{\partial P_e}{\partial_f} \tag{4}$$

Assuming P_e changes linearly with respect to frequency and D equals the percentage change in frequency, the block display of the generator and removal of the feedback branch is shown in Fig. 2.

2.3 Turbine Model

Sources of mechanical power, commonly known as primary propulsion, can consist of water turbines installed in waterfalls and rivers, steam turbines powered by coal or nuclear fuel, as well as gas turbines. The turbine model must relate the changes in mechanical output power to changes in the position of the steam valve. Turbines are very diverse in terms of specification. The simplest primary actuator model is the steam turbine without preheating, a first-class system with time constant T_o, shown as the transfer function in Eq. (5).

$$\frac{\Delta P_m(s)}{\Delta P_v(s)} = \frac{1}{1 + T_o s} \tag{5}$$

The time constant T_o is about 0.3 to 2 s. The transfer function of other types of turbines is much more complex. A block diagram of a simple turbine is shown in Fig. 3.

2.4 Speed Governor Model

When the electric charge of the generator suddenly increases, the power will be more than the mechanical

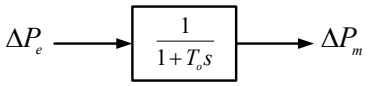

***Fig. 3**: Block diagram of a turbine model.*

power input, and this lack of mechanical power is compensated by the kinetic energy stored in the rotary system. However, the reduction of kinetic energy leads to a decrease in the speed of the turbine and consequently a decrease in generator frequency. The change in speed is felt by the turbine governor which then adjusts the turbine inlet so that the mechanical power of the turbine output increases sufficiently to enable the speed to reach a new permanent state.

For stable operation, the governors are designed to allow the generator to decelerate as the load increases. The speed governor mechanism acts as a comparator. Its input ΔP_g is equal to the difference between the set reference power ΔP_{ref} and the power $1/R\Delta f(s)$.

$$\Delta P_g(s) = \Delta P_{ref}(s) - \frac{1}{R}\Delta f(s) \tag{6}$$

The ΔP_g command is converted to the steering valve position change command via the hydraulic booster. Considering a linear relationship and a T_g time constant for the hydraulic booster, the relationship in Eq. (7) is created in the Laplace domain.

$$\Delta P_v = \frac{1}{1 + T_g s}\Delta P_g \tag{7}$$

2.5 General Model of a Load-Frequency System

By setting the block display in Figs. (1) to (3) and introducing the parameters T_p and K_g, a complete block diagram is achieved for load-frequency control of a separate power system unit, as shown in Fig. 4.

$$K_g = \frac{1}{D}, \qquad T_p = \frac{2H}{f D} \tag{8}$$

2.6 Load-Frequency Control System Response

Since the load change in the power system is usually performed by disconnecting or connecting fixed values, step input is used in the study of load frequency to model the load changes. To analyze the response of the LFC system to a step load change, the speed switch must be first be considered to ensure it is in a certain position $\Delta P_{ref} = 0$.

According to Fig. 4, the output relationship of the control system Δf in the case where $\Delta P_{ref} = 0$ is as follows [21]:

$$\Delta f = \frac{K_p}{1 + T_p s}\left[\frac{-1}{R}\Delta F \frac{1}{\left(1 + T_g s\right)\left(1 + T_o s\right)} - \frac{\Delta P_L}{s}\right] \tag{9}$$

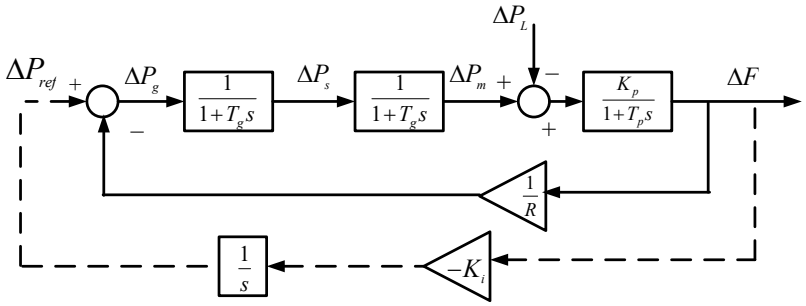

Fig. 4: *Output relationship of the control system.*

Furthermore, according to the theorem, the final value of the system's sustained response is:

$$\Delta f = \lim_{s\to 0}[s\Delta F(s)] = \frac{RK_p}{R+K_p}\Delta P_L = -\frac{\Delta P_L}{\beta} \quad (10)$$

This relationship shows the frequency changes due to variations in load. The denominator of the relationship is defined as the frequency response characteristic of the region (including generator and load) according to

$$\beta = D + \frac{1}{R} \quad (11)$$

As can be seen from Eq. (10), if $\Delta P_{ref} = 0$, the change in frequency will never be zero because D is the load profile and R cannot be too small for stability reasons. In fact, as the system load increases, the turbine speed decreases before the governor can adjust the inlet steam for the new load, which in turn reduces the system frequency. Therefore, the added load is compensated by two components: increasing the output and decreasing the overall load of the system due to a decrease in frequency.

So it is possible that the system frequency does not return to the nominal value. However, if the load of the speed changer varies step by step at the same time as the step change, the response of the control system will change. Therefore, in exchange for changing the load, the speed changer can be controlled so that the final frequency of the system reaches the nominal value.

During normal operation, the actual power exchanged through the communication line is equal to:

$$P_{12} = \frac{|E_1|\cdot|E_2|}{X_{12}}\sin\delta_{12} \quad (12)$$

where $X_{12} = X_1 + X_{tie} + X_2$ and $\delta_{12} = \delta_1 - \delta_2$. Therefore, for small deviations, the transfer power is around the nominal value:

$$\Delta P_{12} = \frac{dP_{12}}{d\delta_{12}}\Delta\delta_{12} = T_{12}\Delta\delta_{120} \quad (13)$$

The quantity T_{12} is the slope of the power angle curve at the nominal operating point $\delta_{120} = \delta_{10} - \Delta\delta_{20}$, known as the power synchronization coefficient, written as:

$$T_{12} = \frac{dP_{12}}{d\delta_{12}} = \frac{|E_1|\cdot|E_2|\cos\Delta\delta_{120}}{X_{12}} \quad (14)$$

Therefore, the power line deviation is as follows:

$$\Delta P_{12} = T_{12}\left(\Delta\delta_1 - \Delta\delta_2\right) \quad (15)$$

By replacing the angle changes with the frequency changes and taking the Laplace transform from both sides, a strong relationship is formed:

$$\Delta P_{12} = \frac{2\pi T_{12}}{s}\left[\Delta F_1 - \Delta F_2\right] \quad (16)$$

Given that the communication line losses have been ignored, $\Delta P_{12} = \Delta P_{21}$ or in terms of pu:

$$\Delta P_{12}S_1 = -\Delta P_{21}S_2 \quad (17)$$

where S_1 and S_2 are the nominal powers of areas 1 and 2 in terms of MVA. The coefficient a_{12} can be defined according to Eq. (18):

$$\Delta P_{21} = a_{12}\Delta P_{12}$$
$$a_{12} = \frac{S_1}{S_2} \quad (18)$$

Entering the transfer power ΔP_{21} in the block view of area 1 gives:

$$\Delta F_1 = \frac{K_{p1}}{1+T_{p1}s}\left[\Delta P_{m1} - \Delta P_{L1} - \Delta P_{12}\right] \quad (19)$$

Similarly, changing the frequency of area 2 gives:

$$\Delta F_2 = \frac{K_{p2}}{1+T_{p2}s}\left[\Delta P_{m2} - \Delta P_{L2} - a_{12}\Delta P_{12}\right] \quad (20)$$

Current power from the communication line appears in the form of increasing load in one area and decreasing load in another. The direction of the power is determined by the difference in angles, i.e., if $\Delta\delta_1 > \Delta\delta_2$ the direction of the current runs from region 1 to region 2. Like the one-area power system, a second control loop is required to eliminate the frequency error. However, as mentioned earlier, in multi-area power systems, the transmittance

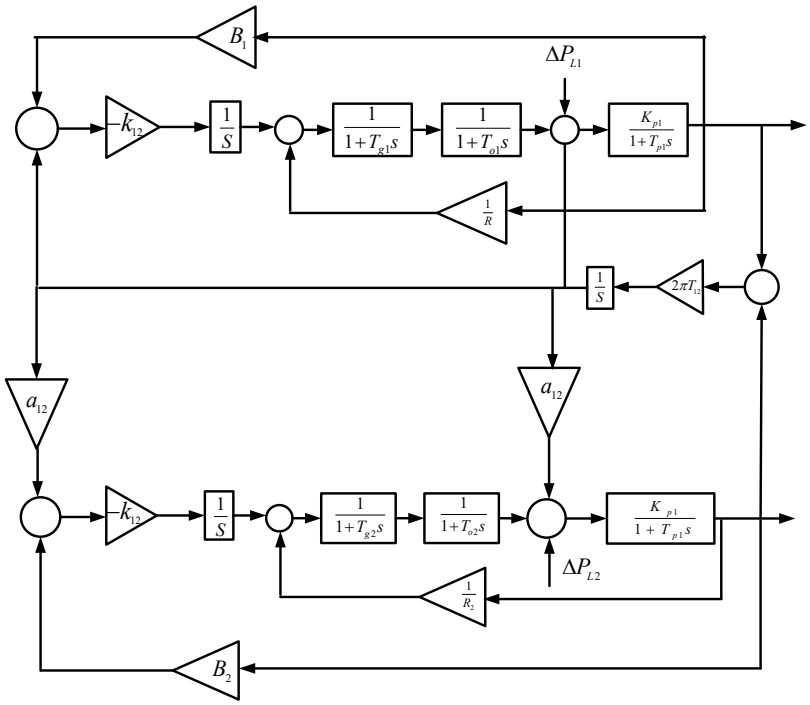

Fig. 5: *Load-frequency control block diagram model of a two-area power system.*

of communication lines in a permanent state must be constant and equal to predetermined values. Therefore, to apply a complete control that satisfies both objectives in addition to frequency changes, the power transmission line changes must be reversed and the linear combination of the two lines be considered as the controller input. This linear combination is called area control error or ACE and defined according to Eq. (21) in each area.

$$\begin{aligned} ACE_1 &= \Delta P_{12} + B_1 \Delta f_1 \\ ACE_2 &= \Delta P_{21} + B_2 \Delta f_2 \end{aligned} \tag{21}$$

Therefore, using an integral controller gives:

$$\begin{aligned} \Delta P_{ref1} &= -K_{i1} \int ACE_1 dt \\ \Delta P_{ref2} &= -K_{i2} \int ACE_2 dt \end{aligned} \tag{22}$$

B is called the frequency bias coefficient of the region and its values are usually equal to β or the frequency response characteristic of each region. A block model of the two-area system is shown in Fig. 5.

3. OPTIMIZATION ALGORITHM

The PID controller is usually implemented according to

$$u(t) = k_p e(t) + \frac{1}{\tau_i} \int e(t')dt' + \tau_d e'(t) \tag{23}$$

In this step, first fuzzy self-regulation is used to obtain the parameters k_p, τ_i, and τ_d with the Ziegler-Nichols (ZN) formulas. These results are used as the initial value of the controller parameters. The system unit step response is then determined by a controller using these initial parameters. Therefore, the output error and rate of change in output error can be obtained. The fuzzy self-adjustment method uses error and error rate change to create the membership functions and fuzzy rules [22–25].

3.1 Fuzzy Tuning Adjustment

In the fuzzy automatic tuning algorithm proposed in this section, the system output is first determined using the ZN method and relay feedback test. By determining the response error and its rate of change and using them as input variables of the fuzzy regulator, the proportional gain and integral time can be found. The rate of change in the output error is obtained by

$$\Delta e(k) = e(k) - e(k-1) \tag{24}$$

Fuzzy automatic regulators calculate $k_p(k)$ and $\tau_i(k)$ using

$$k_p(k) = k_p(k-1) + \Delta k_p(k) \tag{25}$$

$$\tau_i(k) = \tau_i(k-1) + \Delta \tau_i(k) \tag{26}$$

The proportional gain changes $\Delta k_p(k)$ and integral time changes $\Delta \tau_i(k)$ are obtained with an inference from the system output as shown in Fig. 6.

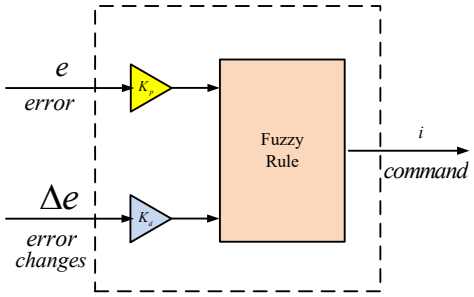

***Fig. 6**: Fuzzy implementation block diagram.*

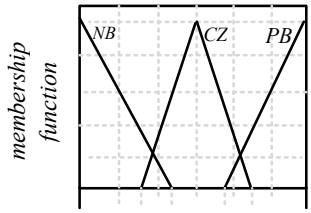

***Fig. 7**: Membership functions.*

3.2 Fuzzy Rule

The rules used in this section to determine $k_p(k)$ and $\tau_i(k)$ include Eqs. (27) and (28):

a) Rule for $\Delta k_p(k)$:

$$R': \text{ if } e(k) \text{ is } A_j \text{ and } \Delta e(k) \text{ is } B_j, \text{ then } \Delta k_p(k) \text{ is } C_{j,i} \tag{27}$$

b) Rule for $\Delta \tau_i(k)$:

$$R': \text{ if } e(k) \text{ is } A_j \text{ and } \Delta e(k) \text{ is } B_j, \text{ then } \Delta \tau_i(k) \text{ is } D_{j,i} \tag{28}$$

where i is the law number.

3.3 Membership Functions for Inputs

The membership functions related to the error input $e(k)$ and the input of the error changes $\Delta e(k)$ are defined using the triangular membership functions shown in Fig. 7.

It should be noted that each epoch has six membership functions.

3.4 Design Fuzzy Rules

Fuzzy language variables are used to construct the fuzzy rules. These rules are designed on the basis that increasing the proportional interest of k_p increases its overlap and decreases the climb time, while increasing the integral time τ_i reduces the climb time. Using the step response error curve, the regulatory rules for k_p and τ_i can be found.

a) Regulatory rules for k_p:

***Table 1**: Fuzzy rules relating to proportional interest.*

$e(k)$	$\Delta e(k)$		
	N	Z	P
N	N	P	N
Z	P	Z	N
P	P	N	P

***Table 2**: Fuzzy rules relating to integral time constants interest.*

$e(k)$	$\Delta e(k)$		
	N	Z	P
N	P	N	P
Z	N	Z	P
P	N	P	N

***Table 3**: Parameters values of the two areas in the system.*

Parameters	Area 1	Area 2
Integral gain constant	$K_{i1} = 0.5$	$K_{i2} = 0.5$
Speed governor time constant	$T_{g1} = 0.08$	$T_{g2} = 0.08$
Turbine time constant	$T_{t1} = 0.3$	$T_{t2} = 0.3$
Proportional gain constant	$K_{p1} = 120$	$K_{p2} = 120$
Power system time constant	$T_{p1} = 20$	$T_{p2} = 20$
Regulation constant	$R_1 = 2.4$	$R_2 = 2.4$
Frequency bias factor	$B_1 = 0.425$	$B_2 = 0.425$
Synchronizing power coefficient	$T_{12} = 0.086$	
Nominal power ratio	$a_{12} = -1$	

- Increase $k_p(k)$ to increase the output.
- Decrease $k_p(k)$ to reduce the output.
- Decrease $k_p(k)$ to reduce the output.
- Increase $k_p(k)$ to increase the output.

The above regulatory rules can be converted to fuzzy rules as shown in Table 1.

b) Regulatory rules for τ_i:

- Decrease $\tau_i(k)$ to increase the output.
- Increase $\tau_i(k)$ to decrease the output.
- Increase $\tau_i(k)$ to decrease the output.
- Decrease $\tau_i(k)$ to increase the output.

The foregoing regulatory rules can be converted to fuzzy rules as presented in Table 2.

4. SIMULATION AND CASE STUDIES

Table 3 shows the specifications of the system under study while the control model of power systems is presented in Figs. 8 and 9.

4.1 Investigation of Fuzzy Controller Results in a Two-Area Power System

The same values as presented in Table 3 are used to compare the parameters of the classical and fuzzy

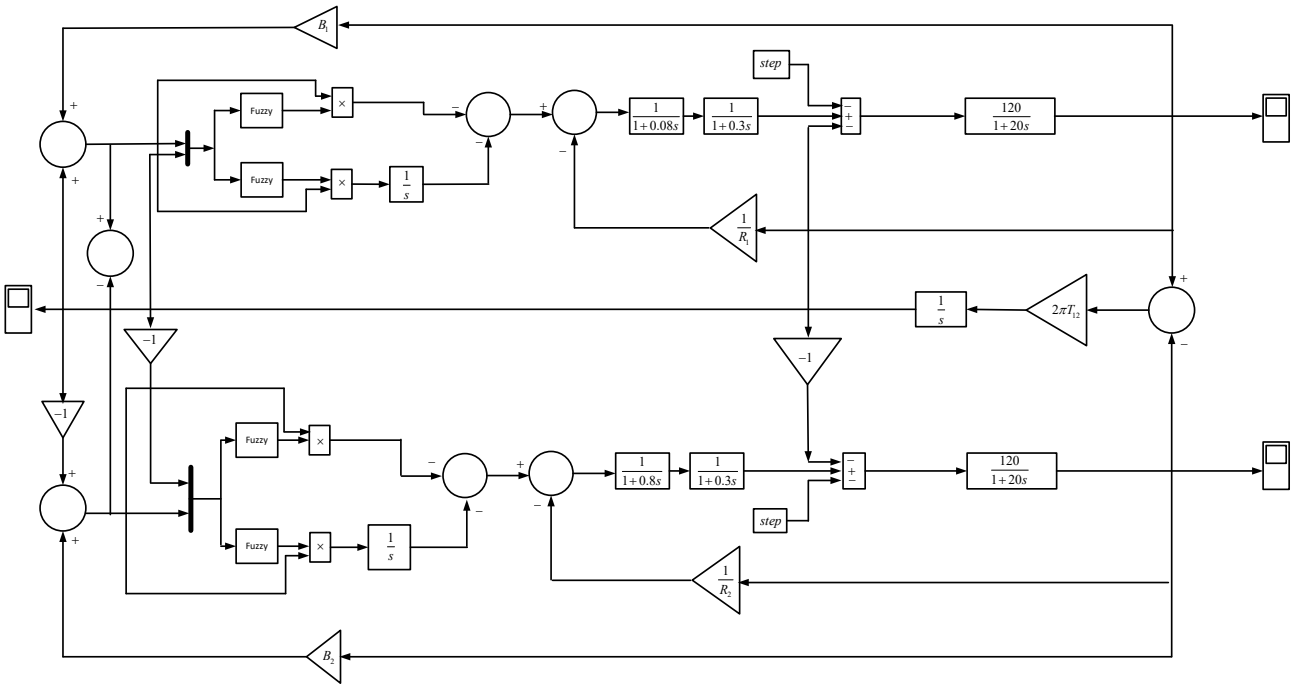

***Fig. 8**: Simulation of load-frequency control in a two-area power system with two inputs for a fuzzy system.*

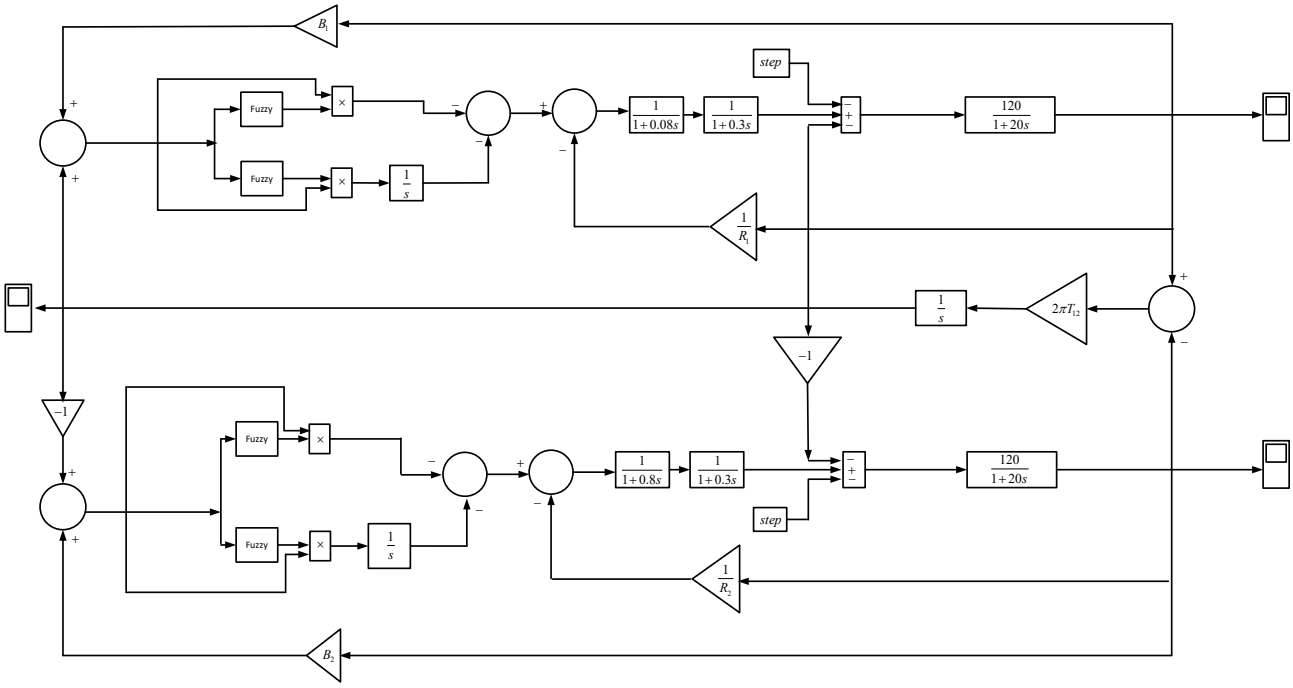

***Fig. 9**: Simulation of load-frequency control in a two-area power system by considering an input for a fuzzy system.*

systems for the two areas of the power system, applying the load change with an input step function of the same amount in area 1.

Firstly, a fuzzy system with two inputs is considered and the frequency changes recorded in areas 1 and 2 as well as the amount of change in transmission power between the two areas (Figs. 10–12).

As can be seen from the figures, both the frequency and changes in transmission power become zero after a while.

4.2 Investigation of Fuzzy and Classical Controller Behavior

The fuzzy load-frequency controller with its classic mode is compared here. To do so, the frequency changes

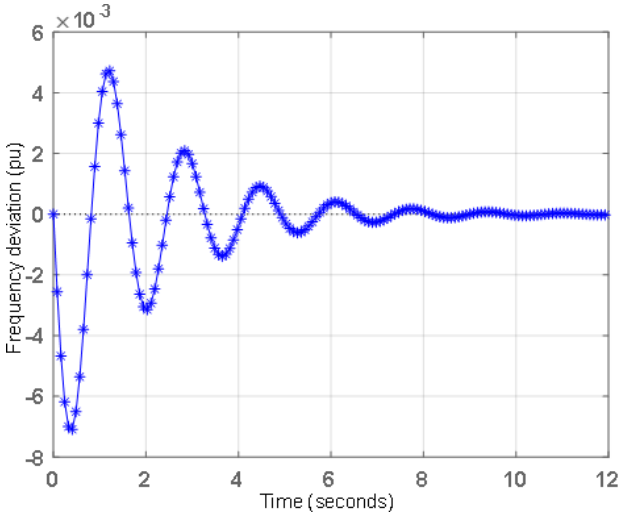

***Fig. 10**: Frequency changes in area 1 to increase the load with two-input fuzzy control.*

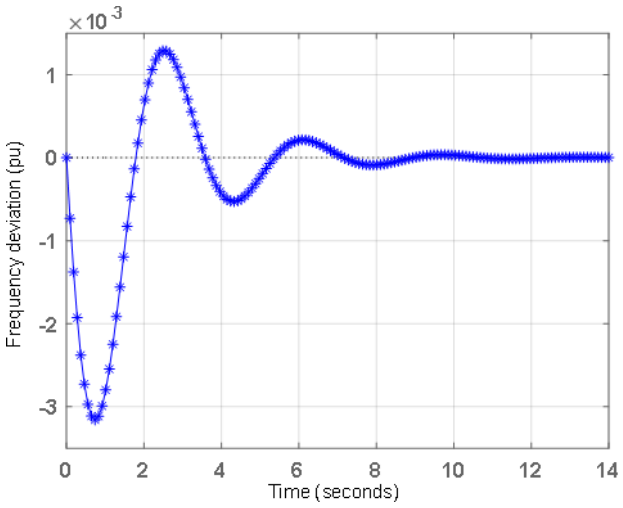

***Fig. 11**: Frequency changes in area 2 for increasing the load in area 1 with two-input fuzzy control.*

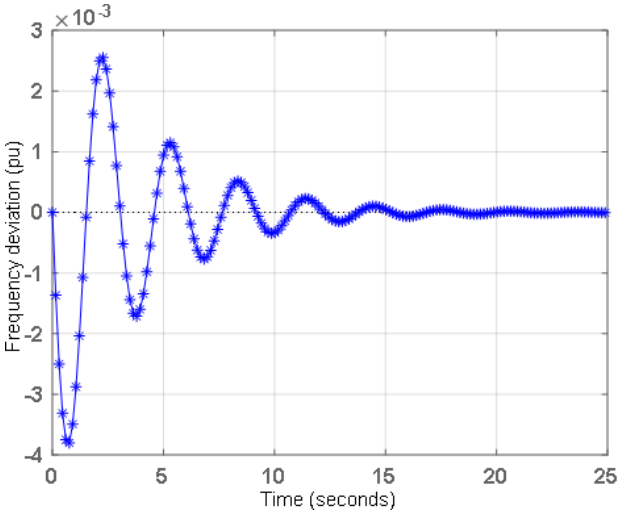

***Fig. 12**: Transmission power changes for areas 1 and 2 with an increasing load in area 1 and two-input fuzzy control.*

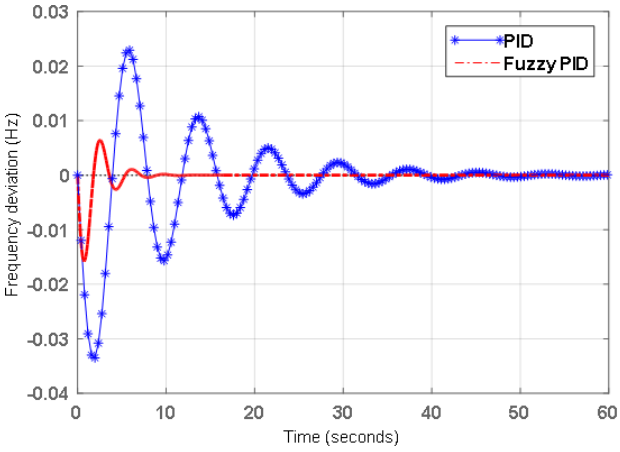

***Fig. 13**: Frequency deviation of the first area with disturbance applications.*

of area 1 in exchange for the load change are compared with a single-input fuzzy controller in classical mode. As can be observed in the figures, the steady-state error for both controllers becomes zero over time, implying the correct operation. However, the main difference between these two controllers is in the transient state of this parameter and when an overload occurs.

This is because, with the classical controller, in the worst possible case, the frequency of area 1 is reduced to 0.021 Hz, and the peak-to-peak frequency change 0.035 pu. Whereas with the fuzzy controller, the frequency is reduced to 0.011 Hz, and the peak-to-peak changes. The frequency deviation is only 0.016 Hz, which is smaller than the classic mode, and since the frequency drop is accompanied by an overall reduction in system load, it can play a significant role in system stability without reducing the system load.

Accordingly, it can be said that the most important advantage of the fuzzy controller in controlling the load frequency of the two-area power system, in addition to maintaining system stability, is that it improves the dynamic behavior of the load-frequency system.

4.3 Comparison of the Proposed Method with Traditional PID

In this section, the frequency changes and their response to disturbances in different areas of the system are examined by reviewing three case studies.

4.3.1 Apply perturbation to the first region and observe the frequency deviation in both regions

The results of the power system are compared with those of a traditional controller. As shown in Fig. 13, despite the perturbation of about 0.1 pu, the frequency deviation in the first area, with the help of a fuzzy controller, is very low and out of control.

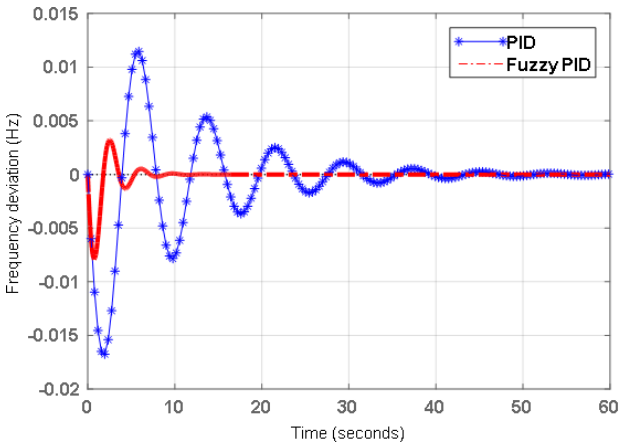

Fig. 14: *Frequency deviation in the second area by disturbing the first area.*

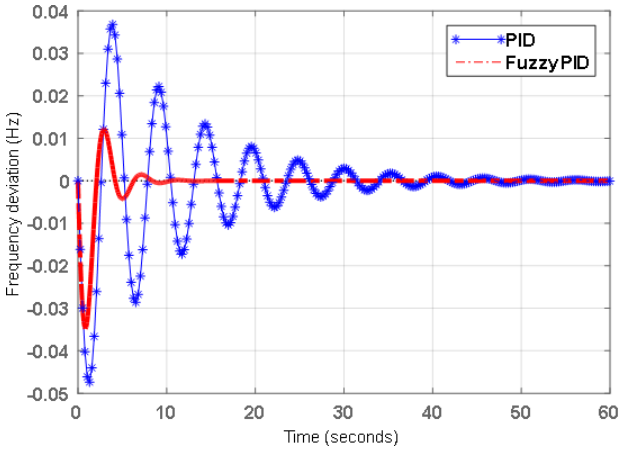

Fig. 15: *Frequency deviation in the second area by disturbing the second area.*

In fact, when the turbulence increases by a stepwise load of 0.1 pu in the first area, the frequency deviation is equal to −0.014 Hz if the fuzzy controller is used. On the other hand, if the fuzzy controller is not used, the changes in frequency are approximately −0.037 Hz, indicating a high probability of instability in the network frequency. In addition, the frequency deviation must be noted at the settling time, which for a system with a fuzzy controller, is approximately equal to 8 s and approximately 48 s for a system without a fuzzy controller.

The performance of the proposed method in controlling the frequency of the power system can be evaluated by applying the disturbance in any of the regions and observing the deviation in frequency. Therefore, the two areas will be confused at the same time, and the frequency deviation of each area observed separately. All the cases can then be compared without controlling the system.

In this section, despite the disturbance applied to the first area, the frequency deviation of the second area can still be observed. Fig. 14 shows that the frequency

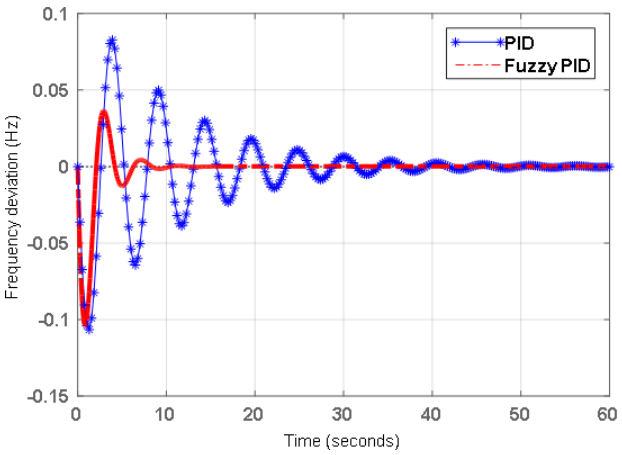

Fig. 16: *Frequency deviation in the first area by disturbing actions in the second area.*

deviation in the first area is less than the second area. However, the frequency deviation in the second region in the two states of the system with and without the fuzzy controller is also noteworthy. In the system with a fuzzy controller, the deflection frequency of the second area is approximately −0.007 Hz, while without a fuzzy controller, the deflection is approximately −0.017 Hz.

4.3.2 Applying disturbance to the second region and observing the frequency deviation in both regions

This section is also aggravated in the form of an increase in the number of 0.1 pu loads in the second application area. First, the deviation in the frequency of the second region in both modes of the system is observed with and without the fuzzy controller.

According to Fig. 15, the results obtained from the application of turbulence to the second region and the deviation of the frequency resulting from it can be seen in the second region. For a system in which a fuzzy controller is used for frequency and load control, the frequency deviation is approximately −0.033 Hz, while in the conventional system, the frequency deviation is approximately −0.047 Hz. The settling time is approximately equal to 9 s with the fuzzy controller and 53 s in conventional mode.

The frequency deviation is examined in the first region, which is the result of turbulence in the second area. It can be observed from Fig. 16 that, with respect to the application of turbulence, when 0.1 pu enters the second region, the frequency deviation of the first region is less than for the second region.

In Fig. 16, the frequency deviation from the application of disturbance to a system using a fuzzy controller is approximately equal to −0.1 Hz, while the settling time for the proposed system is approximately 10 s and 49 s for the conventional system.

The frequency deviation in both regions with respect to the application of disturbances is now investigated.

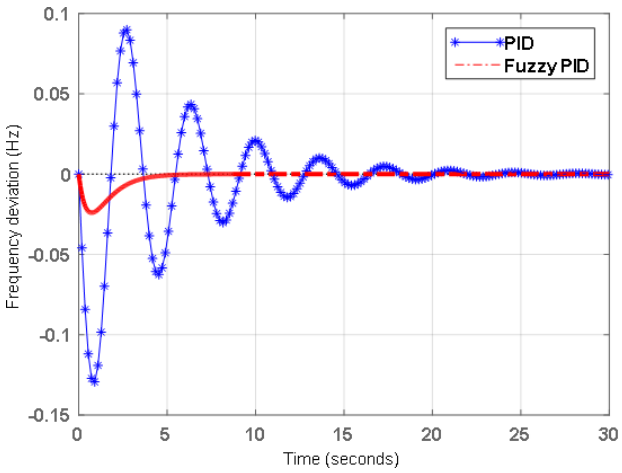

Fig. 17: Frequency deviation in the first area by disturbing the two areas.

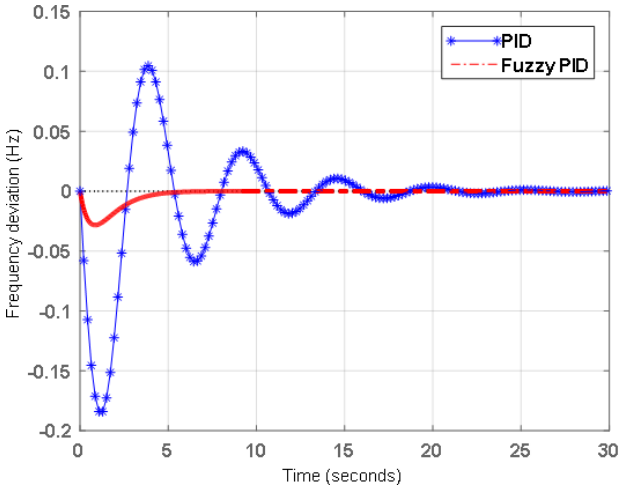

Fig. 18: Frequency deviation in the second area with disturbing actions in both areas.

4.3.3 Applying disturbance to two areas and observing the frequency deviation of each

In this section, the disturbance is studied in the form of a step load increment as 0.1 pu, applied to both areas. As can be observed from Fig. 17, the effect of the turbulence applied to each of the two areas of the system with the fuzzy controller is that the frequency deviation of the first area is approximately equal to −0.021 Hz, and −0.128 Hz in the system. Moreover, the settling time is approximately equal to 5 s with the fuzzy controller and 26 s in conventional mode.

According to Fig. 18, the frequency deviation for the proposed system is approximately −0.030 Hz and −0.171 Hz for the convention system. Besides, the settling time is approximately equal to 4.7 s with the fuzzy controller and 23 s in conventional mode.

There are three basic steps in the fuzzy controller design: 1) cognitive policy, 2) setting control parameters, and 3) membership function determination. In order

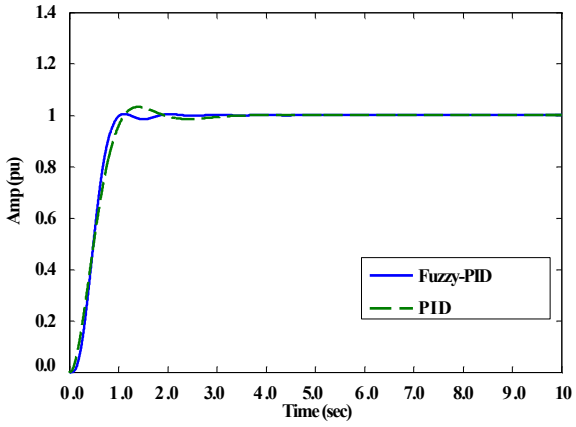

Fig. 19: Output signal amplitude (step response) with PID and the Fuzzy-PID controller.

Table 4: Summary of the simulation results using conventional methods and the Fuzzy-PID controller.

Algorithm	K_p	K_i	K_d	ITAE
Fuzzy-PID	0.689	0.887	0.258	0.481
PID	0.834	0.312	0.764	0.489
Ziegler-Nichols	0.701	0.721	0.124	0.488
Cohen-Coon	0.795	0.415	0.345	0.499

for the fuzzy controller to perform its control objectives correctly, the above steps must be strictly adhered to. In this section, using the integral time-weighted absolute error (ITAE) criterion, a simple test system is examined (represented in [1, 2], part of the AVR controlling block) with optimal adjustment for the PID controller and proposed Fuzzy-PID controller.

Fig. 19 shows the system output signal since ITAE is considered as the objective function to be minimized. As can be observed, the output signal from the proposed controller has lower overshoot, settling time, and less rise time than the PID controller. Table 4 shows a summary of the simulation results.

$$\text{ITAE} = \int_0^T t|e|dt + \int_0^T u^2 dt \tag{29}$$

where e is the error between the reference and output signals, t represents the time, and u is the control signal for each controller.

Although the PID controller is well configured and tuned, the proposed controller response to the changes is more effective. A new scenario is considered in this paper which turns off the connection of area 2 at t = 30 s. The frequencies of those areas are then maintained individually as shown in Figs. 20 and 21.

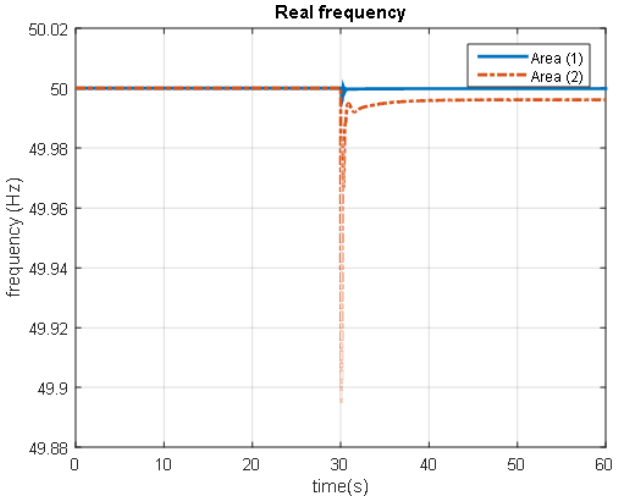

Fig. 20: Real frequency in areas for the turn-off scenario.

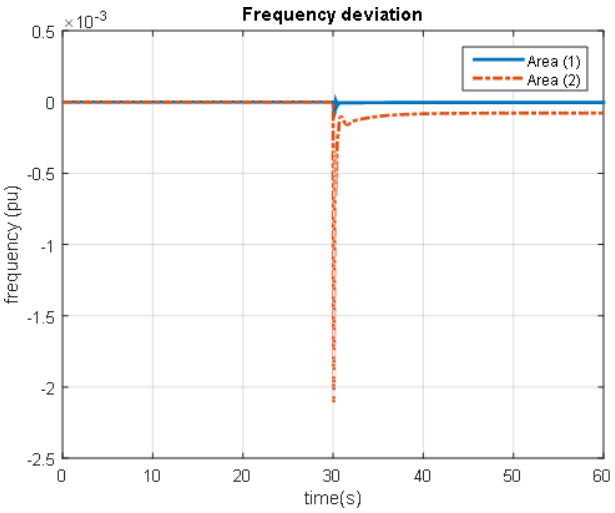

Fig. 21: Frequency deviation in areas for the turn-off scenario.

5. CONCLUSION

The simulation results show that if deviation is applied to any area of the power system, the fuzzy controller is better able to recover the frequency than conventional power system frequency control. In fact, in this way, the efficiency of the above-mentioned method can be developed, and its ability to reduce deviation, frequency, and power in the system observed. In addition, the simulation results and comparisons show that the behavior of the fuzzy controller against load changes shows a greater improvement than the classical controller, along with a robust performance. Correspondingly, the dynamic behavior of the system with the fuzzy controller under different conditions is more favorable than the classical controller. Therefore, it seems that the fuzzy controller is more suitable for practical application. The fuzzy controller is flexible and shows resistance against changing system parameters as well as nonlinear factors such as limiting the production rate under different load change conditions in future projects. For this purpose, a suitable controller should be used in such a way that the connection of these micro-networks is performed at the appropriate time so that the frequency remains within the permitted range. Synchronization in the share of each source and power control by inverters is performed by a fuzzy controller. The proposed controller allows the production resources to be connected to each other with the least fluctuation. This causes the power balance constraint to be observed in transient moments, allowing the frequency control performance to be effective. In independent operation, if the area can supply its own load and due to load changes, the production of electrical power changes in such a way as to supply the requested load at the appropriate frequency, the desired conditions are obtained. However, in the operation of multi-area systems, the effect of frequency changes in each region on adjacent areas must also be studied.

REFERENCES

[1] H. Alhelou, M.-E. Hamedani-Golshan, R. Zamani, E. Heydarian-Forushani, and P. Siano, "Challenges and opportunities of load frequency control in conventional, modern and future smart power systems: A comprehensive review," *Energies*, vol. 11, no. 10, 2018, Art. no. 2497.

[2] Z. Yan and Y. Xu, "Data-driven load frequency control for stochastic power systems: A deep reinforcement learning method with continuous action search," *IEEE Transactions on Power Systems*, vol. 34, no. 2, pp. 1653–1656, Mar. 2019.

[3] C. Chen, M. Cui, X. Fang, B. Ren, and Y. Chen, "Load altering attack-tolerant defense strategy for load frequency control system," *Applied Energy*, vol. 280, Dec. 2020, Art. no. 116015.

[4] M.-H. Khooban, T. Niknam, M. Shasadeghi, T. Dragicevic, and F. Blaabjerg, "Load frequency control in microgrids based on a stochastic noninteger controller," *IEEE Transactions on Sustainable Energy*, vol. 9, no. 2, pp. 853–861, Apr. 2018.

[5] J. Li, T. Yu, and X. Zhang, "Coordinated load frequency control of multi-area integrated energy system using multi-agent deep reinforcement learning," *Applied Energy*, vol. 306, Jan. 2022, Art. no. 117900.

[6] X. Shang-Guan, Y. He, C. Zhang, L. Jiang, J. W. Spencer, and M. Wu, "Sampled-data based discrete and fast load frequency control for power systems with wind power," *Applied Energy*, vol. 259, Feb. 2020, Art. no. 114202.

[7] M.-H. Khooban, T. Dragicevic, F. Blaabjerg, and M. Delimar, "Shipboard microgrids: A novel approach to load frequency control," *IEEE Transactions on Sustainable Energy*, vol. 9, no. 2, pp. 843–852, Apr. 2018.

[8] D. Yu, H. Zhu, W. Han, and D. Holburn, "Dynamic multi agent-based management and load frequency

control of PV/fuel cell/ wind turbine/ CHP in autonomous microgrid system," *Energy*, vol. 173, pp. 554–568, Apr. 2019.

[9] M.-H. Khooban, "Secondary load frequency control of time-delay stand-alone microgrids with electric vehicles," *IEEE Transactions on Industrial Electronics*, vol. 65, no. 9, pp. 7416–7422, Sep. 2018.

[10] H. Zhang, J. Liu, and S. Xu, "H-infinity load frequency control of networked power systems via an event-triggered scheme," *IEEE Transactions on Industrial Electronics*, vol. 67, no. 8, pp. 7104–7113, Aug. 2020.

[11] A. Abbaspour, A. Sargolzaei, P. Forouzannezhad, K. K. Yen, and A. I. Sarwat, "Resilient control design for load frequency control system under false data injection attacks," *IEEE Transactions on Industrial Electronics*, vol. 67, no. 9, pp. 7951–7962, Sep. 2020.

[12] A. Abazari, H. Monsef, and B. Wu, "Coordination strategies of distributed energy resources including FESS, DEG, FC and WTG in load frequency control (LFC) scheme of hybrid isolated micro-grid," *International Journal of Electrical Power & Energy Systems*, vol. 109, pp. 535–547, Jul. 2019.

[13] K. Lu, W. Zhou, G. Zeng, and Y. Zheng, "Constrained population extremal optimization-based robust load frequency control of multi-area interconnected power system," *International Journal of Electrical Power & Energy Systems*, vol. 105, pp. 249–271, Feb. 2019.

[14] H. Luo, I. A. Hiskens, and Z. Hu, "Stability analysis of load frequency control systems with sampling and transmission delay," *IEEE Transactions on Power Systems*, vol. 35, no. 5, pp. 3603–3615, Sep. 2020.

[15] J. Khalid, M. A. Ramli, M. S. Khan, and T. Hidayat, "Efficient load frequency control of renewable integrated power system: A twin delayed DDPG-based deep reinforcement learning approach," *IEEE Access*, vol. 10, pp. 51 561–51 574, 2022.

[16] Z. Wang and Y. Liu, "Adaptive terminal sliding mode based load frequency control for multi-area interconnected power systems with PV and energy storage," *IEEE Access*, vol. 9, pp. 120 185–120 192, 2021.

[17] X.-C. Shangguan, Y. He, C.-K. Zhang, L. Jin, W. Yao, L. Jiang, and M. Wu, "Control performance standards-oriented event-triggered load frequency control for power systems under limited communication bandwidth," *IEEE Transactions on Control Systems Technology*, vol. 30, no. 2, pp. 860–868, Mar. 2022.

[18] K. S. Xiahou, Y. Liu, and Q. H. Wu, "Robust load frequency control of power systems against random time-delay attacks," *IEEE Transactions on Smart Grid*, vol. 12, no. 1, pp. 909–911, Jan. 2021.

[19] M. Gheisarnejad, "An effective hybrid harmony search and cuckoo optimization algorithm based fuzzy PID controller for load frequency control," *Applied Soft Computing*, vol. 65, pp. 121–138, Apr. 2018.

[20] N. Jalali, H. Razmi, and H. Doagou-Mojarrad, "Optimized fuzzy self-tuning PID controller design based on tribe-DE optimization algorithm and rule weight adjustment method for load frequency control of interconnected multi-area power systems," *Applied Soft Computing*, vol. 93, Aug. 2020, Art. no. 106424.

[21] J. R. Nayak, B. Shaw, and B. K. Shahu, "Load frequency control of hydro-thermal power system using fuzzy PID controller optimized by hybrid DECRPSO algorithm," *International Journal of Pure and Applied Mathematics*, vol. 114, no. 9, pp. 147–155, 2017.

[22] X. Jin, K. Chen, Y. Zhao, J. Ji, and P. Jing, "Simulation of hydraulic transplanting robot control system based on fuzzy PID controller," *Measurement*, vol. 164, Nov. 2020, Art. no. 108023.

[23] Y. Wang, Q. Jin, and R. Zhang, "Improved fuzzy PID controller design using predictive functional control structure," *ISA Transactions*, vol. 71, pp. 354–363, Nov. 2017.

[24] D. Somwanshi, M. Bundele, G. Kumar, and G. Parashar, "Comparison of fuzzy-PID and PID controller for speed control of DC motor using LabVIEW," *Procedia Computer Science*, vol. 152, pp. 252–260, 2019.

[25] G. Chen, Z. Li, Z. Zhang, and S. Li, "An improved ACO algorithm optimized fuzzy PID controller for load frequency control in multi area interconnected power systems," *IEEE Access*, vol. 8, pp. 6429–6447, 2020.

Saeed Gerami Moghaddam received his B.S. degree in Electrical Engineering from Islamic Azad University of Bojnord, Iran in 2019. He is currently an M.Sc. student in Islamic Azad university of Kharg, Iran. His research interests include renewable energies, power system, and distribution network.

Ali Asghar Bagheri received his Ph.D. degree in Electrical Engineering from Shiraz University, Iran in 2018. He is an assistant professor in Department of Electrical Engineering, Dashteatan Branch, Islamic Azad University, Dashtestan, Iran. His research interests include renewable energies, wind generation, and power system modelling.

Reza Sedaghati received his Ph.D. degree in Electrical Engineering in 2019. He is an assistant professor in Department of Electrical Engineering, Beyza Branch, Islamic Azad University, Beyza, Iran. His research interests include renewable energies, optimization, FACTS devices and power system dynamics.